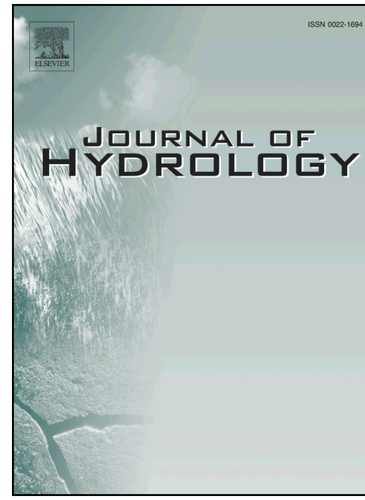

Research papers

Influence of a Subsurface Cut-off Wall on Nitrate Contamination in an Unconfined Aquifer

Qiguo Sun, Tianyuan Zheng, Xilai Zheng, Qinpeng Chang, Marc Walther

PII:	S0022-1694(19)30475-5
DOI:	https://doi.org/10.1016/j.jhydrol.2019.05.030
Reference:	HYDROL 23763
To appear in:	*Journal of Hydrology*
Received Date:	24 January 2019
Revised Date:	6 May 2019
Accepted Date:	8 May 2019

Please cite this article as: Sun, Q., Zheng, T., Zheng, X., Chang, Q., Walther, M., Influence of a Subsurface Cut-off Wall on Nitrate Contamination in an Unconfined Aquifer, *Journal of Hydrology* (2019), doi: https://doi.org/10.1016/j.jhydrol.2019.05.030

Influence of a Subsurface Cut-off Wall on Nitrate Contamination in an Unconfined Aquifer

Qiguo Sun[1], Tianyuan Zheng[2*], Xilai Zheng[1*], Qinpeng Chang[1], Marc Walther[3,4]

1. Key laboratory of Marine environment and ecological education, Ocean University of China, Qingdao 266100, China

2. College of Engineering, Ocean University of China, Qingdao 266100, China

3. Technische Universität Dresden, Faculty of Environmental Sciences, Department of Hydrosciences, Institute for Groundwater Management, Professorship for Contaminant Hydrology, 01062 Dresden, Germany

4. Helmholtz-Centre for Environmental Research – UFZ Leipzig, Department Environmental Informatics, 04318 Leipzig, Germany

Abstract

Due to shallow groundwater tables and easy water availability, many people live in coastal areas. Additionally, alluvial sediments from fluviatile and marine deposits are highly suitable for agricultural use, making coastal settlement even more desirable. However, groundwater nitrate pollution resulting from widespread application of fertilizers creates difficulties for water management officials. Cut-off walls are used to control seawater intrusion into coastal aquifers. However, until now, the effect of cut-off walls on the nitrate contamination of groundwater has been largely unknown. In this paper, the first

*Corresponding author. Tel.: +86 185 6398 0281;
E-mail address: E-mail: zhengtianyuan@ouc.edu.cn
*Corresponding author. Tel.: +86 130 1250 5297;
E-mail address: E-mail: zhxilai@ouc.edu.cn

investigation of the influence of a subsurface cut-off wall on nitrate contamination in groundwater is discussed. Two sets of laboratory experiments--one with and one without a subsurface cut-off wall--were performed to validate the effectiveness of the constructed numerical model. The effects of the subsurface cut-off wall height, distance between the subsurface cut-off wall and the saltwater boundary, and infiltration rates on nitrate distribution and contamination in groundwater were analyzed. Results showed that after the construction of the subsurface cut-off wall, the domain mean velocity decreased, the migration of nitrate pollutants to the saltwater boundary was reduced, and the nitrate-contaminated area expanded. Further, the morphology of the nitrate pollution plumes changed, an indentation appeared directly above the subsurface cut-off wall, the widths of the transition zones increased significantly, and the transition zones became more diffuse as one approached the saltwater wedge. Three indices were developed to quantify the degree of nitrate contamination. The relative height of the subsurface cut-off wall (*H'*) and the nitrate infiltration rate (*Ni*) were the two most significant factors determining the degree of nitrate contamination in groundwater near the subsurface cut-off wall. Therefore, we suggest that subsurface cut-off walls be designed such that their height lies below an experimentally determined critical height; thus reducing the infiltration rate of the contaminants produced during fertilization through water-saving irrigation techniques.

Key words: Nitrate contamination, Subsurface Cut-off wall, Seawater intrusion, Feflow, Tank experiments

Notation

Greek Letters		Roman Letters	
α_k	Density ratio of species *k*	C_k	Mass concentration of species *k* (C_1 for KNO_3, C_2 for NaCl)
β_{ck}	Solute expansion coefficient	C_{ks}	Maximum mass concentration of species *k*
β_L	Longitudinal dispersivity	C_{k0}	Minimum mass concentration of species *k*
β_T	Transverse dispersivity	D	Distance between subsurface cut-off wall and Γs
Γ_b	Bottom boundary	D'	$D' = D/L$, the relative distance between the subsurface cut-off wall and Γ_s
Γ_f	Freshwater boundary	$\boldsymbol{D}_k$	Coefficient of molecular diffusion
Γ_s	Saltwater boundary	$\boldsymbol{D}_m$	Mechanical dispersion tensor
Γ_u	Upper boundary	d	Thickness of the aquifer
$\triangledown$	Gradient vector	$\boldsymbol{e}$	Gravitational unit vector
$\mathcal{E}$	Porosity	H	Height of the subsurface cut-off wall
ρ	Fluid density	H'	$H' = H/d$, the relative height of the cut-off wall;
ρ_0	Freshwater density	h	Hydraulic head

□	Buoyancy coefficient	$\boldsymbol{I}$	Unit vector
Ω	Domain	$\boldsymbol{K}$	Tensor of hydraulic conductivity
		L	The distance between Γ_f and Γ_s
		Nd	Maximum depth of the contamination zone
		Ni	Nitrate infiltration rate
		Ns	Nitrate contaminated area
		Ng	Total dissolved KNO_3 mass in Ω
		Nd'	$Nd' = Nd/d$, the relative maximum nitrate pollution depth
		Ns'	$Ns' = Ns/S$, the relative nitrate contaminated area. S is the area of the domain, which is equal to $L \times d$
		$\boldsymbol{q}$	Darcy velocity of the fluid
		S_0	Specific storage coefficient
		t	Time
		$\boldsymbol{v}$	Velocity
		x	Horizontal spatial coordinate

1. Introduction

Nitrate pollution in groundwater is a severe environmental and hydrogeological problem and has attracted worldwide attention (Hu et al., 2017; Rodriguez-Galiano et al., 2018; Wang et al., 2018). Excess nitrates in the human body are reduced to toxic nitrite and further converted to nitrosamines, which pose a significant threat to human health (Davidson et al., 2017; Rojas Fabro et al., 2015). Therefore, the WHO and some countries have established drinking water standards limiting the maximum concentration of nitrate nitrogen (NO_3^--N) to 10–11.3 mg/L (Radfard et al., 2018). Since the 1960s, a high degree of nitrate pollution in groundwater has been reported globally. In the United States, Burow et al. (2010) conducted a series of statistical analyses on the NO_3^--N content in 5101 wells nationwide and found that the NO_3^--N content in 427 wells exceeded 10 mg/L. Kringel et al. (2016) analyzed 37 groundwater sources in central Africa and found that the average NO_3^--N concentration was 60 mg/L, with the highest concentration reaching 150 mg/L. In China, the average NO_3^--N concentration in the groundwaters of the seven provinces surrounding the Bohai sea reached 11.9 mg/L, with about 34.1% of the groundwater samples exceeding the established limit (Lu et al., 2019; Zhang et al., 1996).

With the economic development of human society and population growth, the degree of coastal groundwater exploitation has significantly increased (Bosello and De Cian, 2014; Werner et al., 2013; Xin et al., 2016), leading to a decrease in underground water levels and an increase in seawater intrusion (SI) (Bosello and De Cian, 2014; Ferguson and Gleeson, 2012; Singh, 2015). Different engineering approaches have been adopted to alleviate and eventually prevent SI, such as pumping hydraulic barriers, water injection barriers, artificial recharge, and cut-off walls (Abdoulhalik and Ahmed, 2017a; Ahmed, 2017; Allow, 2012; Botero-Acosta and Donado, 2015; Hussain et al., 2015). Cut-off walls can be further categorized into full-section cut-off walls, subsurface cut-off walls, and suspended cut-off walls (Abdoulhalik et al., 2017). Among these, the subsurface cut-off wall is the most common type used in engineering (Abdoulhalik and Ahmed, 2017b; Luyun et al., 2009). The subsurface cut-off wall is embedded into the impervious bottom layer of an aquifer. An opening at the top of the aquifer blocks the saltwater and allows inland freshwater discharge to the ocean (Abdoulhalik and Ahmed, 2017b; Allow, 2012). The effectiveness of subsurface cut-off walls against SI has been widely investigated (Ishida et al., 2003; Kaleris and Ziogas, 2013; Luyun et al., 2009). However, few studies have been concerned with the influence of subsurface cut-off walls on the groundwater flow field and groundwater pollution.

In coastal areas with agricultural and animal husbandry land, nitrate is the pollutant found in the highest concentrations in groundwater.(Du et al., 2011; Rajmohan et al., 2009; van den Brink et al., 2007). Many investigations of contaminant transport in coastal aquifers have been conducted via laboratory experiments (Zhang et al., 2002, 2001) and numerical simulations (Shammas and Thunvik, 2009; Volker et al., 2002; Xin et al., 2019). These investigations indicate that the contaminant transport processes are significantly influenced by variable density flow, sea-level rise, aquifer heterogeneity and stratigraphy, density of the contaminant, and tidal oscillations. However, the number of investigations of nitrate migration in coastal aquifers under the effect of the subsurface cut-off wall is insufficient. Yoshimoto et al. (2013) found that the average concentrations of NO_3^--N in groundwater were below 10 mg/L before the construction of a cut-off wall, and the concentration reached 10 mg/L after the cut-off wall construction. They developed a numerical model that estimated that the NO_3^--N concentration would continue to rise by 0.79-1.46 mg/L over the following 100 years. Lalehzari and Tabatabaei (2015) found that the construction of a subsurface cut-off wall affected the groundwater level upstream of the wall by 4 km, but the NO_3^--N concentration did not change significantly. Kang and Xu (2017) monitored the nitrate concentrations of the groundwater upstream and downstream of a subsurface cut-off wall and found that the average nitrate concentration in the groundwater upstream was 9.92 mg/L, which was much higher than the 0.76 mg/L measured downstream. Overall, the previous studies have found that the construction of a subsurface cut-off wall influences the water level and nitrate concentration in the groundwater upstream of the cut-off wall. However, the spatial distribution of the nitrate concentration in the presence of a cut-off wall has not been considered, and the effects of a subsurface cut-off wall on the prevention of SI and nitrate contamination have not been quantitatively evaluated. Further, the effect of a subsurface cut-off wall on inland pollution and SI has not been explored.

Hence, in our study, we: (1) investigate the influence of a subsurface cut-off wall on the flow field, nitrate distribution, and seawater distribution in an unconfined coastal aquifer; (2) evaluate the effects of the cut-off wall height, distance between the cut-off wall and the saltwater boundary, and nitrate infiltration rates on groundwater nitrate contamination; (3) propose a new optimized construction scheme for cut-off walls that can control SI and reduce the nitrate contamination in groundwater. A variable-density flow and transport model (Feflow 7.0) is applied to investigate nitrate migration and distribution in an unconfined coastal aquifer. Two sets of laboratory experiments--with and without a cut-off wall--were performed to validate the effectiveness of the numerical model. The validated model was then used to predict the degree of nitrate contamination under various conditions.

2. Experimental methods

2.1 Description of the experimental set-up

The laboratory seepage device included a seepage chamber, a salt-freshwater level control system (described below), and a pollution source simulation system (Fig. 1). The dimensions of the central seepage chamber were 1.00 m × 0.60 m × 0.10 m, and the freshwater and saltwater chambers were located on either side of the chamber. Two hard perforated plastic plates with a metal screen on each surface were inserted between the seepage chamber and the water chambers to prevent the artificial aquifer medium from flowing out of the seepage chamber. Two submersible pumps were connected to the inlet holes through silicone hoses to feed the system with water, and the outflow holes were connected with silicone hoses to discharge water to maintain constant freshwater and saltwater levels. In this way, the salt-freshwater water level control system was constructed. The pollution source simulation system consisted of two nitrate-solution distribution pipes and two peristaltic pumps (KCP-C, Kamoer). The distribution pipes were made of rigid plastic pipe (diameter 1 cm × length 20 cm), closed at the end, and into each pipe ten uniformly distributed holes were drilled (bore diameter of 1.5 mm, spacing interval of 2 cm). The pipes were embedded in the surface of the seepage chamber beside each other, and the peristaltic pump controlled the water input and the nitrate infiltration rate.

2.2 Experiment materials

White quartz sand with an effective particle size of 0.5-1.2 mm was used as the aquifer medium. The water samples used were freshwater, saltwater, and a pollutant solution. Freshwater used in the experiment was taken directly from the tap in the laboratory. Saltwater was prepared by dissolving commercial sodium chloride and red food dye in tap water to obtain concentrations of 36.16 g/L and 1.5 g/L, respectively. The pollutant solution was prepared by dissolving KNO_3 in distilled water to a KNO_3 concentration of 0.725 g/L, resulting in a NO_3^--N concentration of 100 mg/L. The prepared solutions were stored in three 75 L plastic buckets. A 0.01 m-thick rigid foam plastic was used as the material for the cut-off wall.

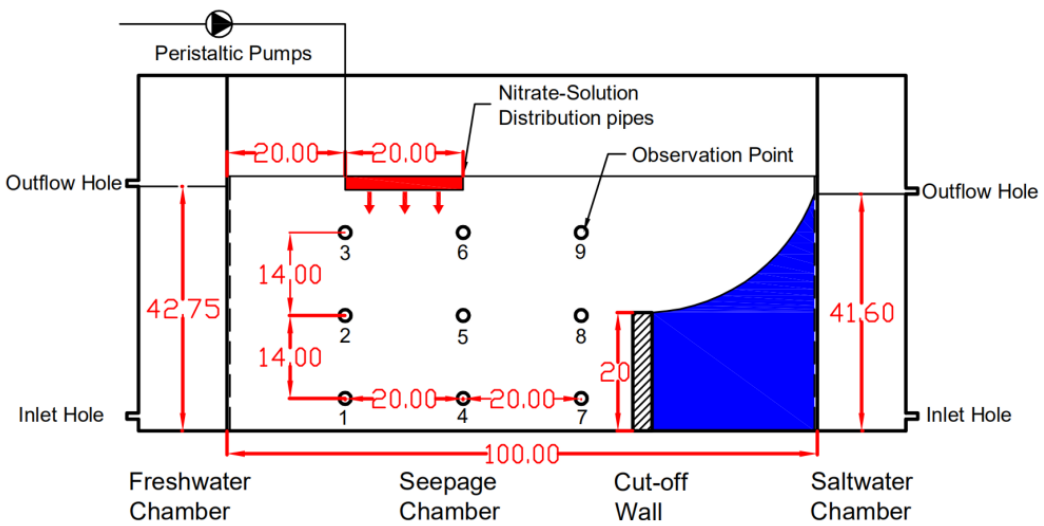

Fig. 1 Schematic diagram of experiment setup; values are in cm.

2.3 Experimental procedure

The experiments included a control, which did not have a subsurface cut-off wall, and a lab-scale model, which did. A summary of the experimental parameters is presented in Table 1. The experimental results were compared with the numerical model to validate the effectiveness of the model setup. First, the seepage chamber was filled with layers of quartz sand; each layer was saturated with water and compacted. Next, nine needles were inserted into the positions corresponding to each observation point shown in Fig. 1. The densities of the KNO_3 and NaCl solutions were measured by a densitometer (DA-300WG, DahoMeter) to be 1025 g/L and 1004 g/L, respectively. The hydraulic conductivity was estimated based on Darcy's law under the constant-head condition and found to be 300 m/d.

The experiments were carried out successively. In the first experiment, SI conditions without the cut-off wall were assumed. In the following experiment, SI conditions and the presence of the subsurface cut-off wall were assumed. At the start of each experiment, freshwater was injected, saturating the entire porous medium with freshwater. Next, the submersible pump in the saltwater bucket was activated to feed the system with saltwater and promote seawater intrusion. When the saltwater level was stable at 41.60 cm, the two peristaltic pumps responsible for the nitrate pollution were activated, and the flow rate of each pump was adjusted to 0.96 m^3/h. In the experiments without a cut-off wall, when the displacement of the saltwater wedge (SW) fell below 0.5 cm over 1 h, a steady state was considered to have been reached, the length of the SW was recorded, and water samples were withdrawn from the nine observation points. In the experiment with a subsurface cut-off wall, the water samples from the nine observation points were extracted every 30 min. When the NO_3^--N concentrations at all observation points remained constant, a steady state was considered to have been reached and the experiment was terminated.

The NO_3^--N concentrations in the water samples were measured using a spectrophotometer (UNICO UV2800A) (Hu et al., 2017). The experimental results are compared to the numerical results below.

3. Numerical model

3.1 Model conceptualization

A vertical cross-section of the groundwater flow and nitrate pollution plume contained by the cut-off wall (Ω) are shown in Fig. 2. The left boundary is the freshwater boundary (Γ_f), corresponding to h_1, the constant hydraulic head of the freshwater flow; the right boundary is the saltwater boundary (Γ_s), corresponding to h_2, the constant hydraulic head of the NaCl flow (NaCl concentration C_{2s} is constant). L denotes the distance from Γ_s to Γ_f. The left and right boundaries of the flow with constant nitrate concentration C_{1s} and variable nitrate infiltration rate *Ni* (m/d) across the top boundary are denoted by x_1 and x_2, respectively. The remaining part of the top boundary (Γ_u) and the bottom boundary (Γ_b) are impervious to water and solutes. The thickness of the aquifer is denoted by d. The height of the subsurface cut-off wall is H, and its distance from Γ_s is denoted by D. For the sake of simplicity, the denitrification process is not considered, because this process does not occur on the laboratory-scale.

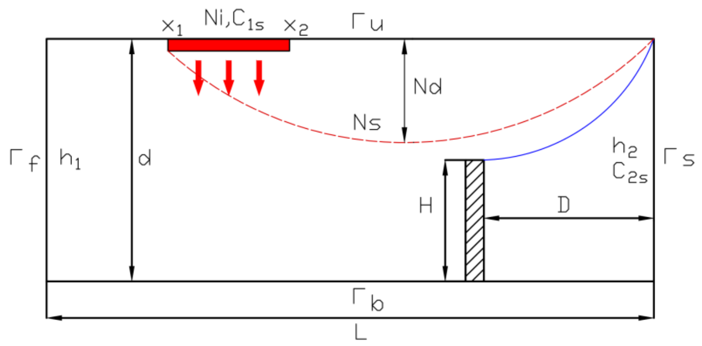

Fig. 2 Conceptualization of the unconfined aquifer near the cut-off wall.

3.2 Mathematical Methods

We model the density-dependent flow and mass transport processes by considering a cross-section of a coastal aquifer using the convective forms of the transport equations. Neglecting the Forchheimer and Brinkman effects, the momentum balance is governed by the Darcy equation in the form:

$$\boldsymbol{q} = -\boldsymbol{K}\left(\nabla h + \chi \boldsymbol{e}\right)$$

As we operated the experiments under constant controlled temperature conditions, we can neglect the influence of temperature on buoyancy and assume that it only depends on the density of species *k*, giving:

$$\chi = \left(\rho - \rho_0\right)/\rho_0 = \sum_k \beta_{ck}\left(C_k - C_{k0}\right)$$

The solute expansion coefficient β_{ck} is defined by

$$\beta_{ck} = \alpha_k / \left(C_{ks} - C_{k0}\right)$$

The continuity equation for mass flow in steady state is given by:

$$S_0 \frac{\partial h}{\partial t} + \nabla \cdot \boldsymbol{q} = 0$$

The mass transport process is described by an advection-dispersion equation:

$$\varepsilon \frac{\partial C_k}{\partial t} + \boldsymbol{q} \cdot \nabla C_{\boldsymbol{k}} - \nabla \cdot \left(D_k \cdot \nabla C_k\right) = 0$$

where ε is the porosity, and the hydrodynamic dispersion tensor $\boldsymbol{D}_k$ is defined by:

$$\boldsymbol{D}_k = \varepsilon D_k \boldsymbol{I} + \boldsymbol{D}_m$$

$\boldsymbol{D}_m$ is the mechanical dispersion tensor, which is a function of the velocity $\boldsymbol{v}$:

$$\boldsymbol{D}_m = \beta_T \left\|\boldsymbol{v}\right\| \boldsymbol{I} + \left(\beta_L - \beta_T\right) \frac{\boldsymbol{v} \otimes \boldsymbol{v}}{\left\|\boldsymbol{v}\right\|}$$

For the initial and boundary conditions, we refer the reader to the guide book of FeFlow (Diersch, 2014).

3.3 Model setup

FEFLOW 7.0 software has been widely used to solve variable-density mass transport problems (Diersch, 2014), and we used it to study the influence of the subsurface cut-off wall on the distribution and degree of nitrate pollutants in groundwater over time. The domain (1.00 m × 0.40 m) was discretized using the advancing front method into 16,960 triangular finite element cells. The diameter of each element was less than 0.94 cm, and the longitudinal and transverse dispersivity values were set to 0.001 m and 0.0001 m, respectively, which are within the range of the dispersivity values presented by Abarca and Prabhakar Clement (2009). The elements in the area occupied by the cut-off wall were considered to be inactive. The fully implicit forward Euler/backward Euler (FE/BE) method was used for simulation-time control, with the time-step size set to 0.001 d and the initial time-step length set to 1×10^{-8} d. The full upwinding method was used in the model. The density-dependent flow transport equations led to symmetric and non-symmetric matrices. Preconditioned conjugate-gradient (PCG) was used to solve the symmetric linear system, and preconditioned and post-conditioned BiCGSTAB was used to solve the non-symmetric linear system. The Picard iteration scheme was used for solving the nonlinear system.

The values of the parameters in the numerical models were consistent with the experimental parameters, which can be found in Table 1. *Ni* was set to 2.3 m/d, and a KNO_3 concentration of 725 mg/L led to a NO_3-N concentration of 100 mg/L The hydraulic conductivity was set to 300 m/d. Nine observation points that were consistent with the positions of the experimental observation points were chosen.

Table 1

Numerical and experimental parameters

Input parameter	Value	Units
Porosity, ε	0.4	-
Freshwater level, h_1	42.75	cm
Saltwater level, h_2	41.60	cm
Freshwater density, ρ_0	1.000	g/cm^3
Saltwater density, ρ_1	1.025	g/cm^3
KNO_3 density, ρ_2	1.004	g/cm^3
Saltwater concentration, C_{2s}	35 000	mg/L

KNO_3 concentration, C_{1s}	725	mg/L
KNO_3 infiltration rate, Ni	2.3	m/d
Hydraulic conductivity, K	300	m/d
Specific storage coefficient, S_0	0.0001	1/m
Longitudinal dispersivity, β_L	0.001	m
Transverse dispersivity, β_T	0.0001	m
Molecular diffusion coefficient	1×10^{-9}	m^2 /s
Density ratio, α_{NaCl}	0.025	-
Density ratio, α_{KNO3}	0.004	-

3.4 Model validation

A plot of the experimental versus the simulated NO_3^--N concentrations at the 9 observation points in steady state is presented in Fig. 3. It is evident that the simulated and observed NO_3^--N concentrations exhibited good correlation, with a root-mean-square error of 1.0152 mg/L. The simulated length of the SW (50.6 cm) and the experimental length of the SW (50.0 cm) agreed well.

Fig. 4 contains a plot of the experimental and simulated NO_3^--N concentrations over time at selected observation points for the scenario with the subsurface cut-off wall. Observation points 1, 2, 4, and 7 did not exhibit nitrate accumulation. Observation point 9 was discarded because the process of sand excavation and refilling disturbed the in-situ state, thus making the experimental result inaccurate. At the other four observation points (3, 5, 6, 8), the experimental and simulated NO_3^--N concentrations agreed well, with an average significant correlation coefficient (R^2) of 0.92253, indicating that the FEFLOW model can be successfully used to simulate nitrate migration and contamination in a coastal aquifer.

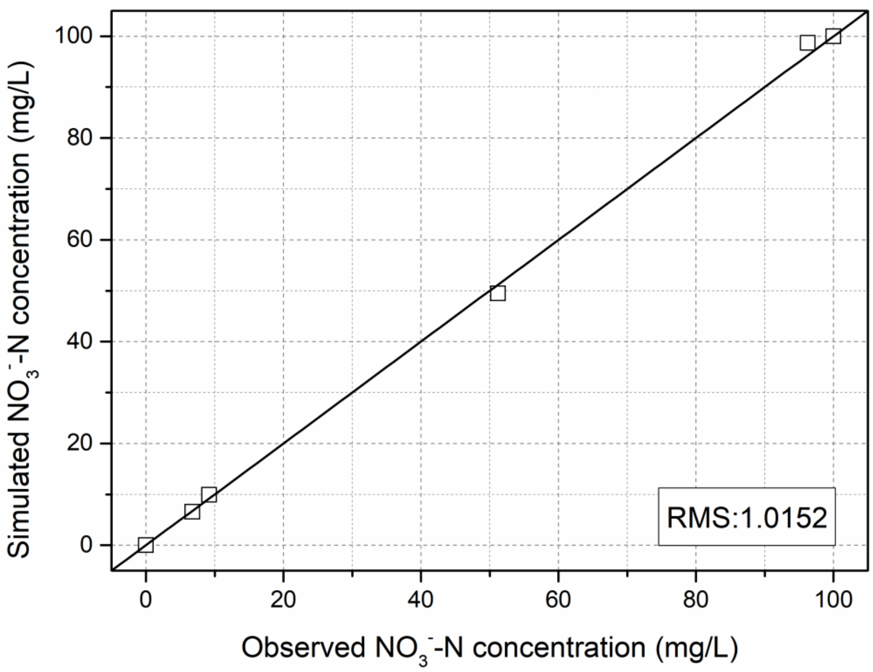

Fig. 3 Comparison of simulated and observed NO_3^--N concentrations in steady-state under the condition of SI at nine observation points. The black line represents perfect (1:1) correlation.

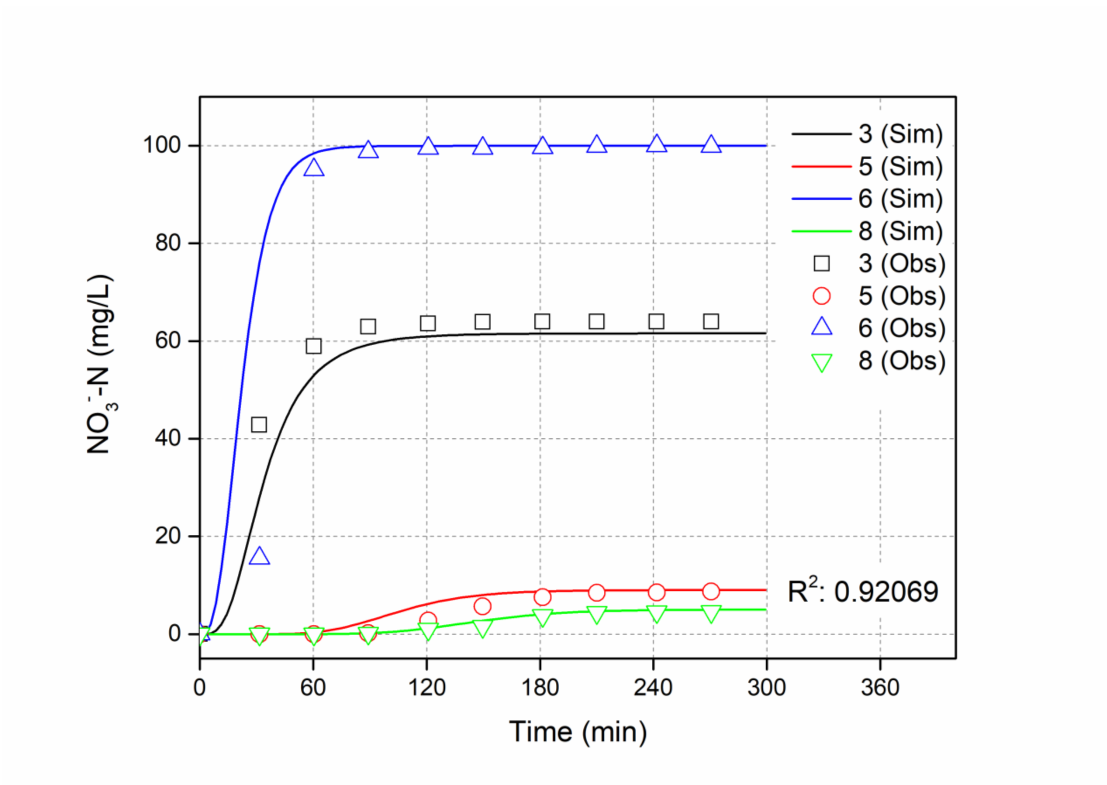

Fig. 4 Comparison of simulated and observed NO_3^--N concentrations over time at selected observation points (3, 5, 6, 8).

3.5 Simulation procedure

In total, four sets of 32 simulations were performed using the validated model to investigate the degree of nitrate contamination in the groundwater after the construction of the subsurface cut-off wall. In the first set of simulations, two groups were considered: those with and those without the subsurface cut-off wall. In the former group, the relative heights of the subsurface cut-off wall (*H'*) equaled 62.5% of the thickness of aquifer, and the relative distances between the cut-off wall and the saltwater boundary (*D'*) were 30%. The nitrate infiltration rate (*Ni*) for both groups was 2.3 m/d. In the second set of simulations, cases with 10 different *H'* values and the same *D'* and *Ni* values as above were considered. In the third set of simulations, cases with 9 different *D'* values, an *H'* of 50%, and the same *Ni* as above were considered. The fourth set of simulation included cases with 11 different *Ni* values, an *H'* of 50%, and a *D'* of 30%. Other parameters used in the simulations were the same in all sets and are presented in Table 1. The influence of the subsurface cut-off wall on nitrate contamination in groundwater was evaluated within each of the four sets of simulation.

4. Results and discussion

4.1. Evaluation methods

Hu et al. (2005) used the Indicator Kriging method with a semivariogram model to assess nitrate contamination in groundwater using a threshold of 20 mg/L NO_3^--N to filter the raw data. The spatial distribution range of nitrate is a common index used to evaluate the degree of nitrate contamination (Chen et al., 2010; Srivastava and Ramanathan, 2018). In this study, a NO_3^--N concentration of 10 mg/L was used as the threshold, which is within established drinking water standards (NO_3^--N to 10–11.3 mg/L) established by the WHO and many countries (Radfard et al., 2018). The area enclosed by the 10 mg/L concentration contour and the upper boundary was defined as the nitrate contamination area. Three pollution-evaluation indexes were proposed: the maximum depth of the contamination zone *Nd* (m) (Fig. 2); the nitrate contaminated area *Ns* (m^2) (Fig. 2); and the total dissolved KNO_3 mass in Ω *Ng* (g). Some of the indices and variables were transformed to dimensionless form:

Nd' = Nd/d, the relative maximum nitrate pollution depth;

Ns' = Ns/S, the relative nitrate contaminated area. *S* is the area of the domain, which equals *L×d*;

H' = H/d, the relative height of the subsurface cut-off wall;

D' = *D/L*, the relative distance between the subsurface cut-off wall and Γ_s.

4.2. Influences of SI and the subsurface cut-off wall on nitrate contamination

4.2.1. Nitrate contamination under the condition of SI without the subsurface cut-off wall

The nitrate solution and saltwater have different densities and exist simultaneously in the domain. To better understand the distribution of the nitrate pollutant, the flow fields before and after the construction of the cut-off wall were analyzed. Fig. 5a shows the flow field under the condition of SI. A low-velocity zone (< 1 m/d) formed in the region occupied by the SW, because the velocity inside the SW region was slow compared to the surface velocity (Chang and Clement, 2013). There was saltwater circulation within the SW region (Smith, 2004), and a vertical flow component formed on the interface that carries the mass upward against the vertical gravitational force (Post et al. 2007). The vertical flow component combined with the horizontal velocity component, making the freshwater and mass migrate along the interface of the SW region. As the height of the SW region increased and its boundary migrated towards the discharge zone, the flow velocity accelerated (Fig. 5a). The maximum flow rate, with a value of 18.95 m/d, appeared near the discharge zone, and the mean velocity of the domain was 2.24 m/d.

In the steady state, a semi-elliptic nitrate pollution plume (Fig. 5c) was formed in the upper portion of the aquifer. *Nd'* and *Ns'* were 52.50% and 33.82%, respectively. The NO_3^--N concentration was the highest (> 90 mg/L) around the nitrate-infiltration zone, and a narrow transition zone was formed at the edge of the plume. Zhang et al. (2002) found that density was the main factor that influenced the shape of the pollution plume; when it was low, the contaminated zone was mainly concentrated in the upper portion of the aquifer with a relatively sharp outline. This is consistent with our observations that the boundary of the nitrate contamination plume was very sharp. We also observed that the pollution plume was contained in the upper portion of the aquifer, because the density of the KNO_3 solution used was only 1.004 g/cm^3.

4.2.2. Nitrate contamination with the use of a subsurface cut-off wall

Fig. 5b shows the flow field patterns after construction of the subsurface cut-off wall (*H'* = 62.5%; *D'* = 30%). The SW was completely blocked outside the cut-off wall, the low-velocity area on the left side of the cut-off wall disappeared, and a small high-velocity zone formed directly above the cut-off wall. A fan-shaped zone characterized by increasing velocity formed around the discharge zone. The area of the low-velocity (1 m/d–2 m/d) zone on the left side of the cut-off wall enlarged, and the mean velocity decreased to 1.93 m/d.

The nitrate migration ability decreased with the decrease in mean velocity, which cause the nitrate-contaminated area to expand and *Nd'* and *Ns'* to increase to 54.68% and 34.58%, respectively. The NO_3^--N average concentration in the upstream aquifer increased from 24.23 mg/L to 25.25 mg/L. A similar trend was reported in Yoshimoto et al. (2013). Due to the action of the high-velocity flow above the cut-off wall, the pollution plume became concave, the width of the nitrate transition zone increased significantly, and the nitrate pollution plume became more diffuse where it approached the saltwater interface (Fig. 5d). The latter observation is consistent with the findings of Zhang et al. (2002), who reported that the front of the plume always becomes more diffuse as it approaches the saltwater interface.

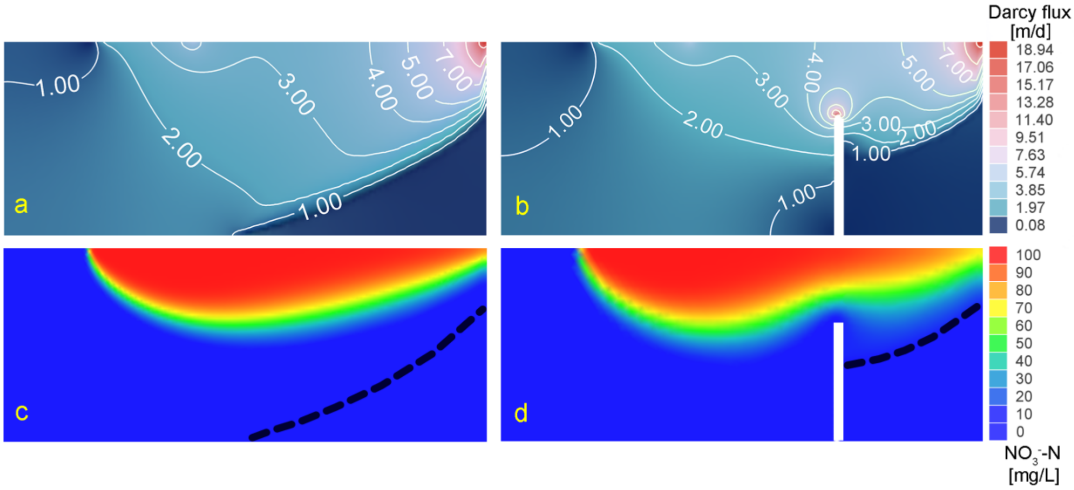

Fig. 5 Comparison of flow fields under the conditions of (a) SI with no subsurface cut-off wall and (b) SI with the subsurface cut-off wall. (c) and (d) show the nitrate distributions under the same SI conditions as (b) with no subsurface cut-off wall and with the subsurface cut-off wall, respectively. The 50% saltwater concentration contour is denoted by the dark blue dashed line.

4.3. Influence of subsurface cut-off wall height on nitrate contamination

The change in *H'* significantly impacted the dimensions of the nitrate-contaminated area (see below), but it did not cause a notable change in the seawater-contaminated area (Fig. 6). When *H'* was 50% (Fig. 6a) and 60% (Fig. 6b), the nitrate pollution plumes were mainly concentrated in the upper portion of the aquifer, the transition zones were narrow, and the total mass of dissolved KNO_3 (*Ng*) hardly changed (Fig. 7). As *H'* was increased to 80% (Fig. 6c), the nitrate-contaminated area expanded, and *Ng* increased to 33.23 g. The thickness of the low-concentration transition zone above the saltwater region increased noticeably. When *H'* was further increased to 90% (Fig. 6d), *Nd'*, *Ns'*, and *Ng* substantially increased to 81.50%, 55.95%, and 45.25 g, respectively. In this case, the aquifer was severely contaminated by nitrate.

The curve of the change in the mean velocity in the domain with *H'* was parabolic (concave down) (Fig. 8), which means that the velocity decreased as the cut-off wall height increased. Wu et al. (2016) found that this crossing velocity was the major factor affecting the extent of nitrate migration in saturated zones, and that the vertical pollution depth increased with decreased crossing velocity. When the cut-off wall was tall, the flow velocity rapidly decreased, which ultimately led to a rapid increase in *Nd'* and *Ns'* in the aquifer (Fig. 9) as *H'* increased. When *H'* was lower than 65%, *Nd'* and *Ns'* increased slowly as *H'* increased, with *Ns'* increasing by 0.94% on average for a 10.00% increase in *H'*. *Nd'* and *Ns'* began to increase more rapidly with respect to an increase in *H'* starting at *H'*=0.65. In the region 0.65<*H'*<0.8, *Ns'* increased by 7.20% on average for a 10.00% increase in *H'*. However, when *H'* was higher than 80%, *Nd'* and *Ns'* increased rapidly with respect to an increase in *H'*, with *Ns'* increasing by 13.98% on average for a 10.00% increase in *H'*. We thus denoted *H'* = 0.8, i.e., the height of the cut-off wall when it is equal to 80% of the thickness of the aquifer, as the critical height. We conclude that cut-off walls should be designed to be less than or equal to the critical height in order limit the nitrate-contaminated area in groundwater aquifers.

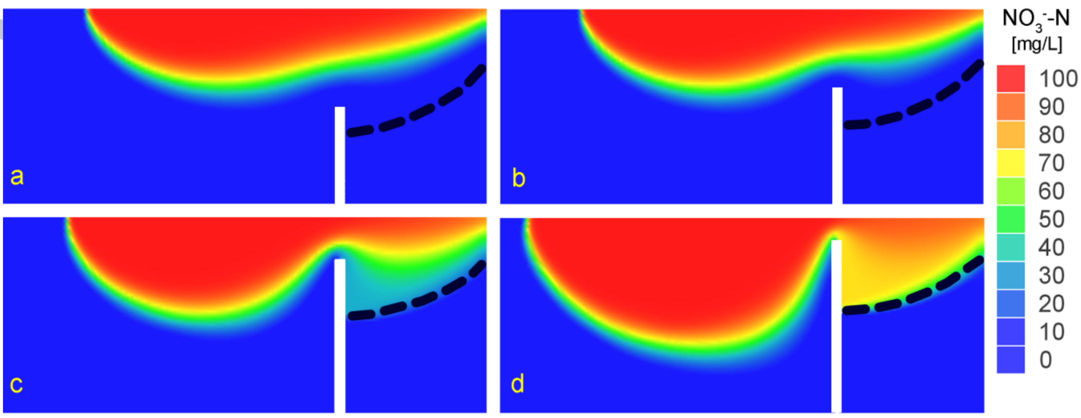

Fig. 6 Steady-state nitrate and saltwater distribution at different relative heights of the subsurface cut-off wall (*H’*): (a) 50%; (b) 60%; (c) 80%; and (d) 90%. The 50% saltwater concentration contour is denoted by the dark blue dashed line.

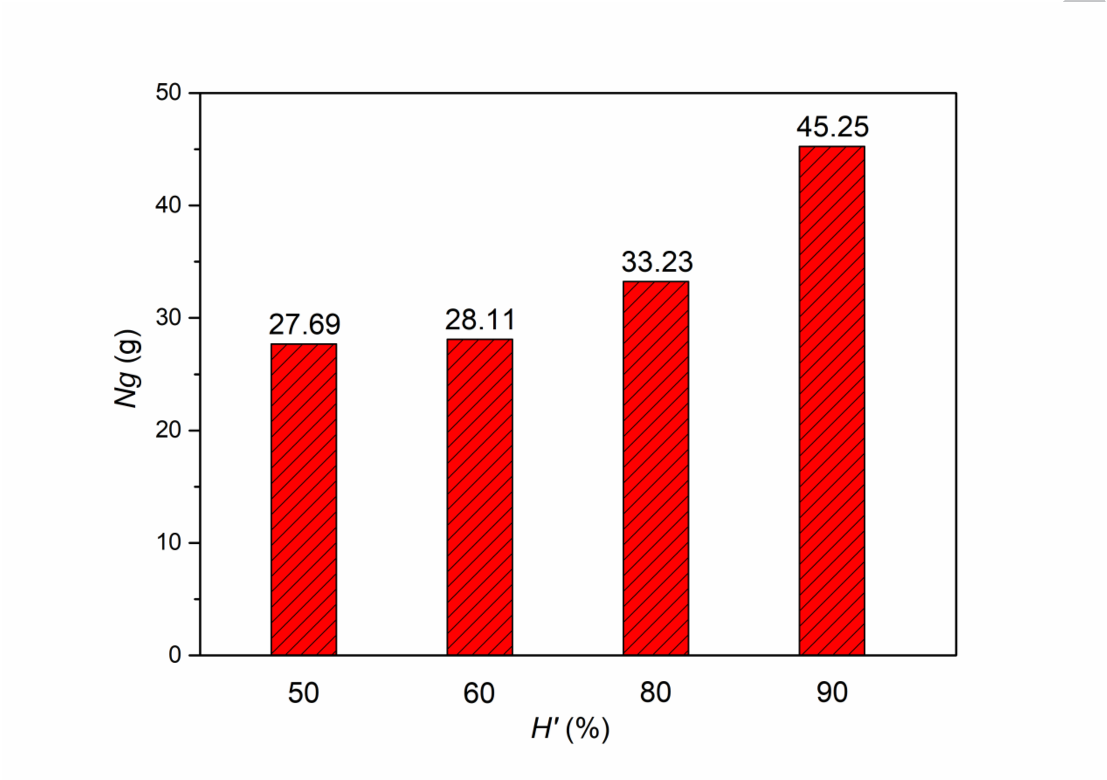

Fig. 7 The total dissolved KNO_3 mass (*Ng*) under steady-state conditions at different relative heights of the subsurface cut-off wall (*H’*).

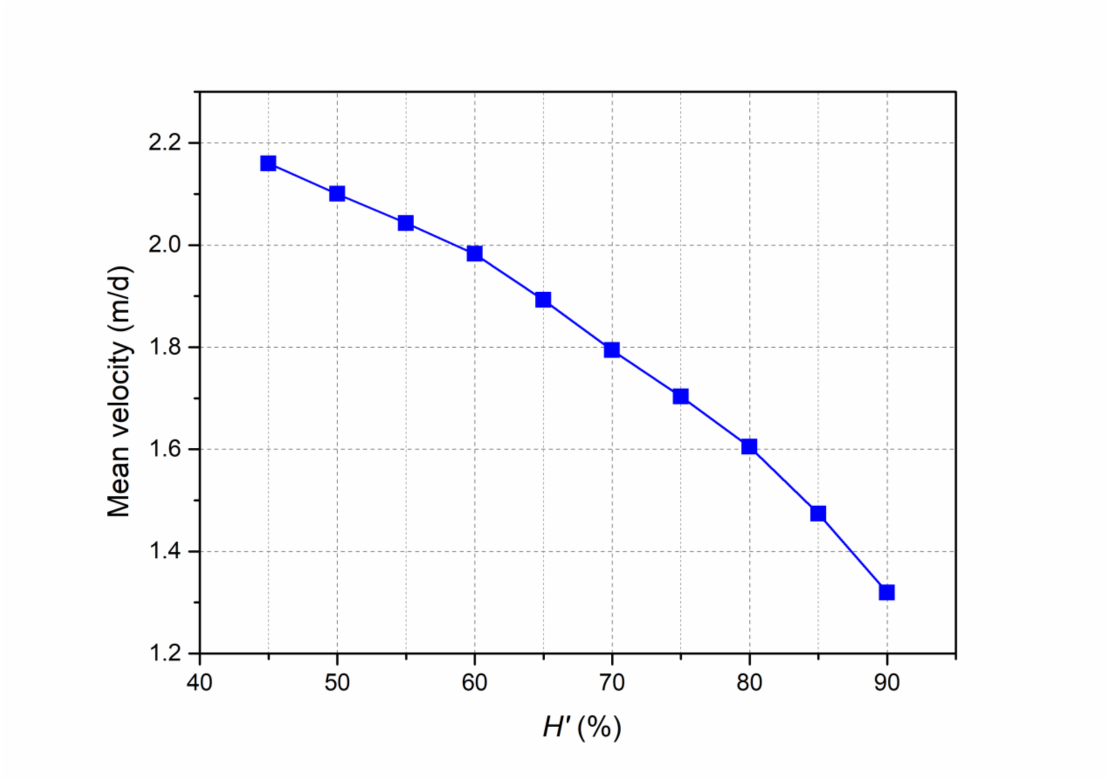

381 Fig. 8 Mean velocity in the domain at different *H'*.

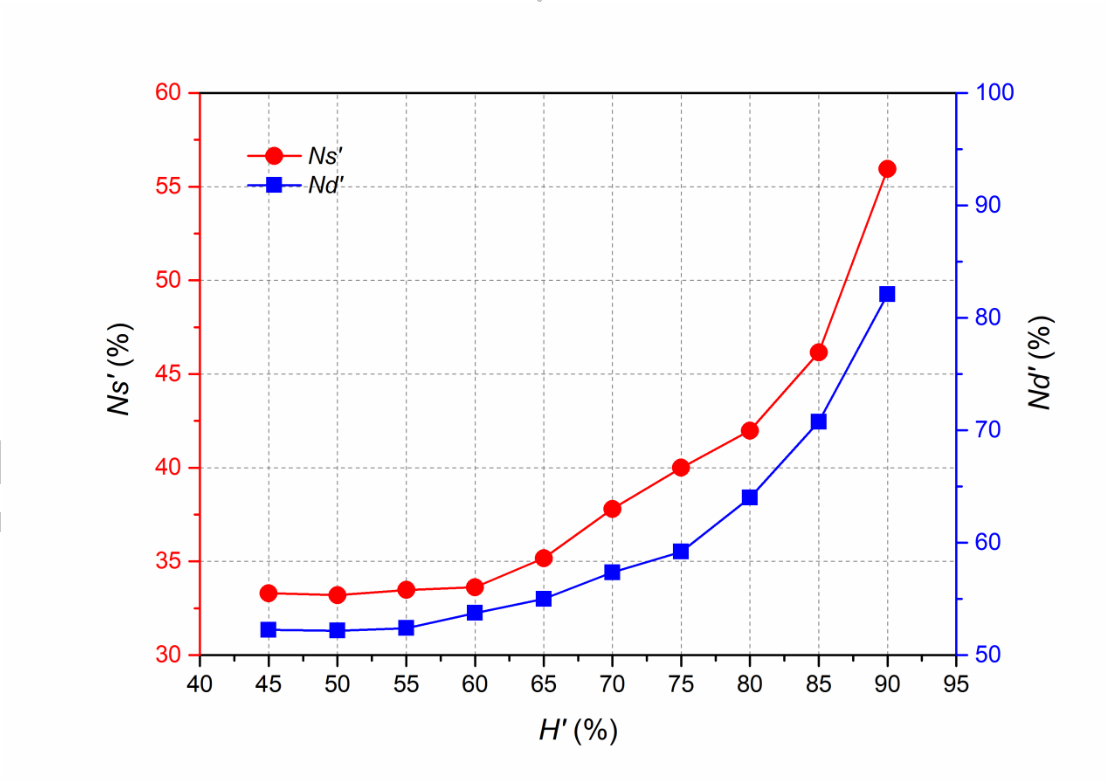

383 Fig. 9 The relative maximum steady-state nitrate pollution depth (*Nd'*) and the relative

384 nitrate contaminated area (*Ns'*) at different *H'*.

4.4. Influence of the distance between the subsurface cut-off wall and the saltwater boundary on nitrate contamination

Change in the relative distance between the subsurface cut-off wall and Γ_s (*D'*) had little impact on the distribution of the nitrate pollutant but influenced the saltwater-contaminated area significantly. Specifically, the saltwater intruded further with increasing *D'* (Fig. 10). When *D'* was increased from 15% to 35%, *Ng* hardly changed (Fig. 11) and *Ns'* decreased very slightly (Fig. 12). *Nd'* tended to decrease with increases in *D'* because the concave configuration maintained a fixed distance from the cut-off wall; as the distance between the cut-off wall and *Nd* decreased, *Nd'* decreased. Overall, the changes in *D'* had little impact on the distribution of the nitrate pollutant. We note that the closer the cut-off wall was to the saltwater boundary, the taller the cut-off wall needed to be to maintain its effectiveness in controlling SI; this increased *Ns'* indirectly. Therefore, we suggest that cut-off walls be constructed at positions such that the lowest possible cut-off wall height that can still control SI be less than or equal to the critical height. In this way, the dual purposes of controlling SI and reducing nitrate contamination can be achieved simultaneously.

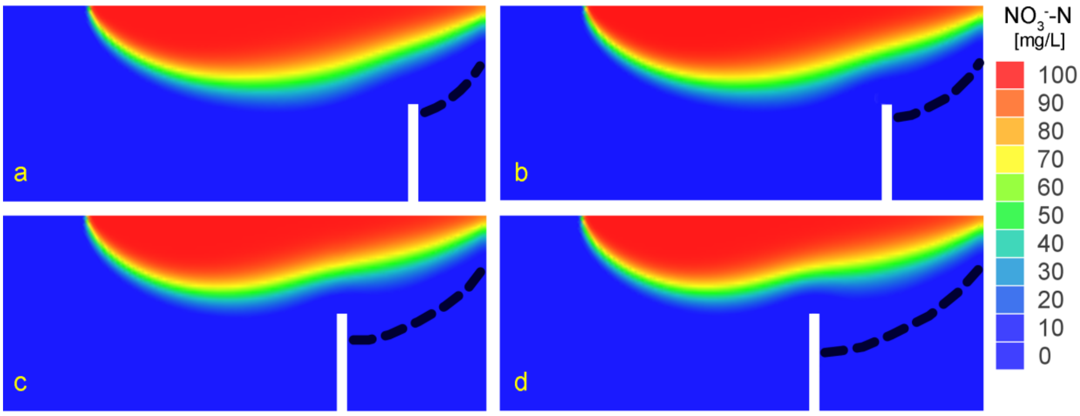

Fig. 10 Steady-state nitrate and saltwater distribution corresponding to different relative distances between the subsurface cut-off wall and Γ_s (D'): (a) 15%; (b) 20%; (c) 30%; (d) 35%. The 50% saltwater concentration contour is denoted by the dark blue dashed line.

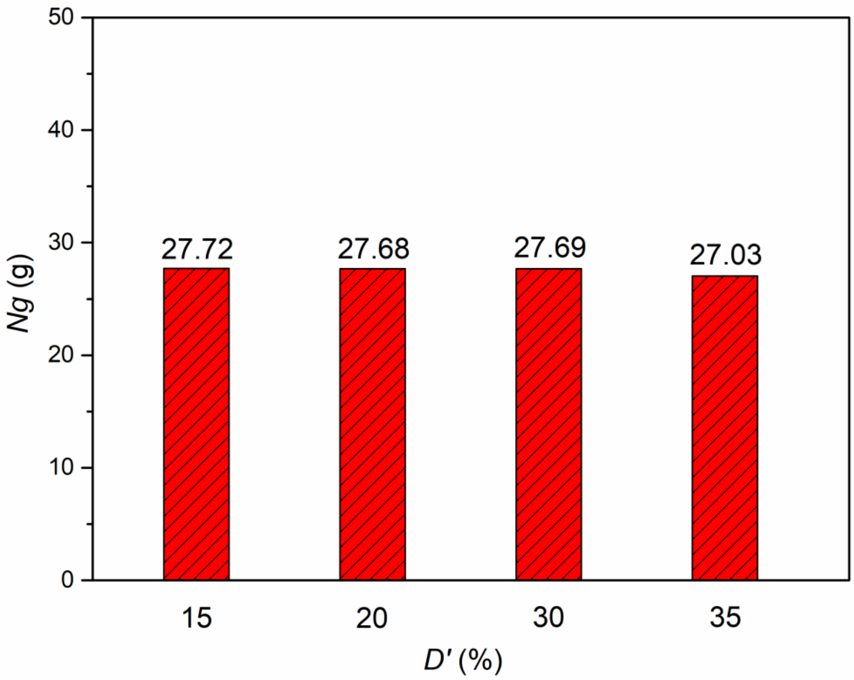

Fig. 11 Steady-state total dissolved KNO_3 mass (Ng) at different relative distances between the subsurface cut-off wall and Γ_s (D').

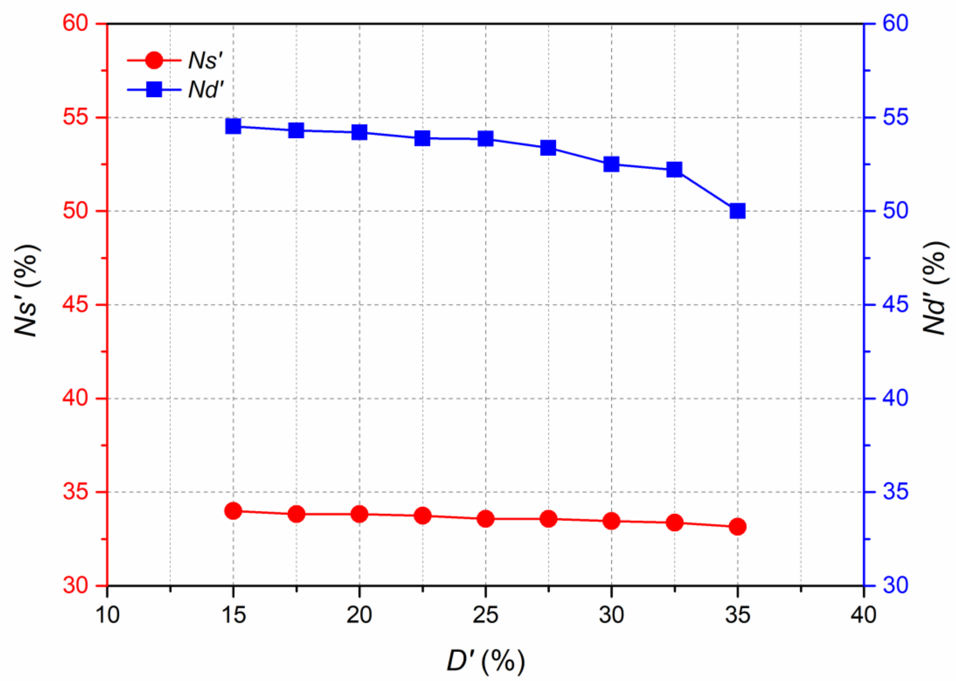

Fig. 12 Steady-state relative maximum nitrate pollution depth (*Nd'*) and the relative nitrate contaminated area (*Ns'*) at different *D'*.

4.5. Influence of infiltration rate on nitrate contamination with subsurface cut-off wall

Fig. 13 shows the influence of *Ni* on the distribution of nitrate and saltwater in steady state. The changes in *Ni* had little effect on the saltwater-contaminated area. When Ni was low, the nitrate pollution plume was distributed along the upper portion of the aquifer in an elongated ellipse (Fig. 13a). As *Ni* (< 2.78 m/d) increased from 1.38 m/d to 2.3 m/d, *Ng* increased from 16.18 g to 21.79 g (Fig. 14), with a 10% increase in *Ni* leading to a 10.67% increase in Ng. With an increase in the infiltration rate, the depth to which the nitrate pollution reached increased noticeably. When the nitrate infiltration rates were 3.45 m/d (Fig. 13c) and 3.68 m/d, *Ng* values were 45.01 g and 49.71 g, respectively. For a 10% increase in *Ni*, *Ng* increased by 15.66% on average. *Ng* increases were more rapid with respect to increases in *Ni* when the latter value was more than 2.76 m/d. In all cases, the nitrate contaminated area expanded to the upstream aquifer.

As can be seen from Fig. 15, the infiltration rate played a decisive role in the vertical migration of the nitrate pollutant. *Nd'* increased linearly with respect to increases in *Ni*, with every 10% increase in *Ni* leading to an average increase in *Nd'* of 4.12%. When *Ni* was lower than 2.76 m/d, *Ns'* increased linearly, with an increase of 2.74% on average for a 10% increase in *Ni*. However, when *Ni* was greater than 2.76 m/d, the curve of *Ns'* versus *Ni* had positive acceleration, leading to an average increase in *Ns'* of 4.28% for a 10% increase in *Ni*. *Ni* was identified as the main factor influencing the distribution of nitrate in groundwater; thus, reducing the infiltration rate during fertilization through water-saving irrigation would be an effective way to prevent expansion of the area of nitrate contamination in groundwater near a subsurface cut-off wall.

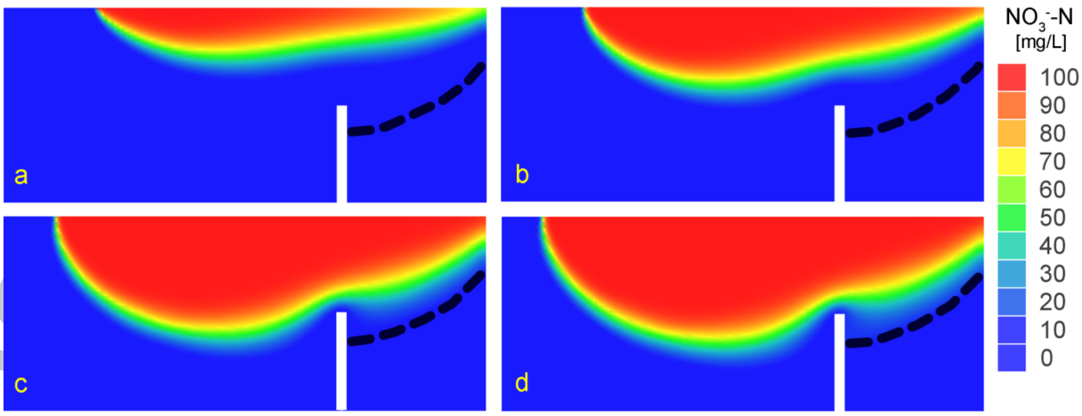

Fig. 13 Steady-state nitrate and saltwater distributions at different nitrate infiltration rates (*Ni*): (a) 1.38 m/d; (b) 2.3 m/d; (c) 3.45 m/d; (d) 3.68 m/d. The 50% saltwater concentration contour is denoted by the dark blue dashed line.

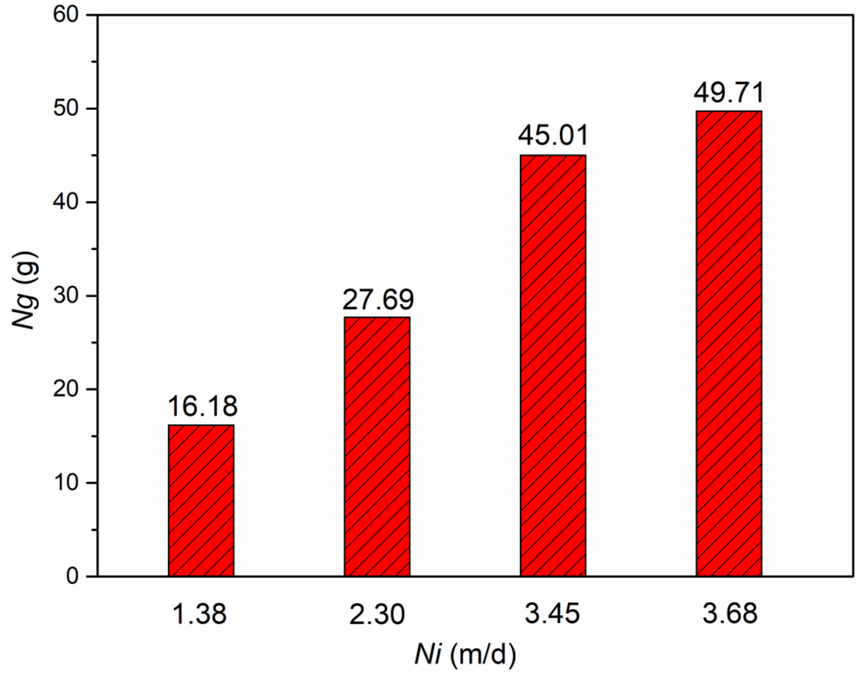

441
442
443 Fig. 14 Steady-state total dissolved KNO_3 mass (*Ng*) at different nitrate infiltration rates
444 (*Ni*).
445

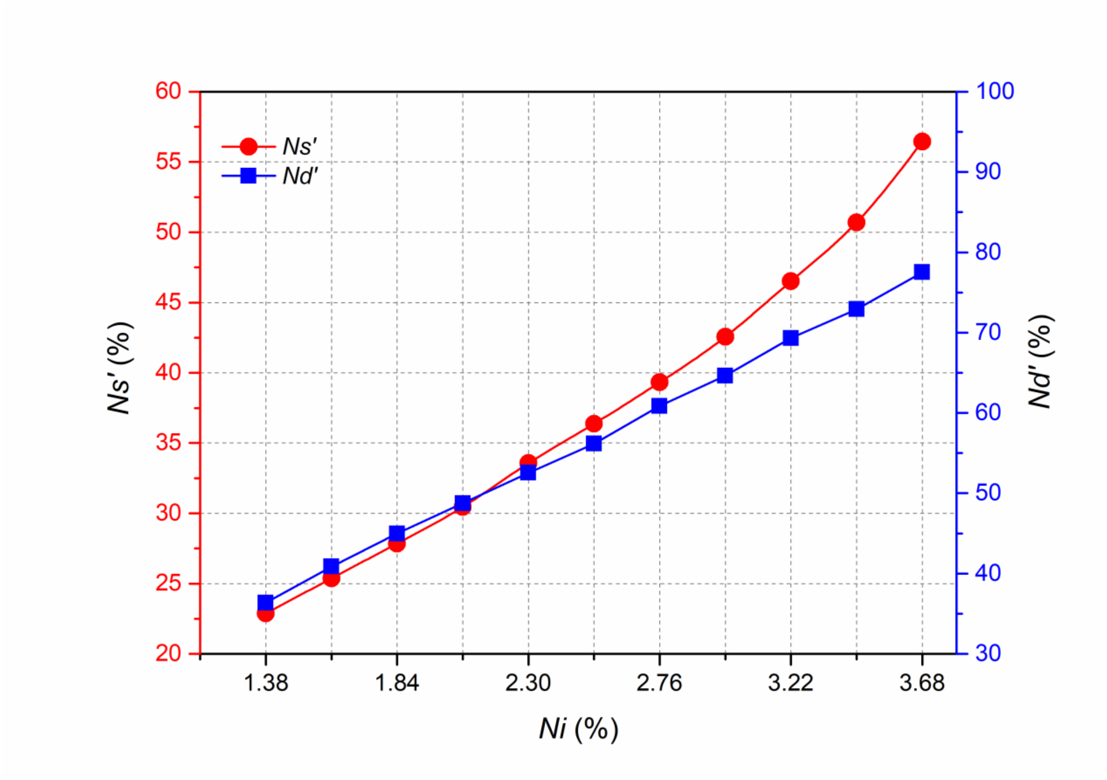

Fig. 15 Steady-state the relative maximum nitrate pollution depth (*Nd'*) and relative nitrate contaminated area (*Ns'*) at different *Ni*.

5. Conclusion

In this study, we used numerical simulations to investigate the influence of a subsurface cut-off wall on nitrate contamination in steady state in a model coastal aquifer. Three indices (*Nd'*, *Ns'*, and *Ng*) were used to analyze the influences of changes in *H'*, *D'*, and *Ni* on nitrate distribution and contamination in groundwater resources. Fig. 16 shows an overall comparison of the sensitivity of the parameters: when *H'* was lower than 65%, *Ns'* increased slowly, with an increase of 0.26% on average for a 10.00% increase in *H'*. there is an elevated increase starting from *H'*>65%, due to an accelerated increase in *Ns'* with respect to increases in *H',* this parameter increased by 5.28% on average for a 10.00% increase in *H'*. *D'* had very little impact on *Ns'*. *Ns'* linearly increased with respect to an increase in *Ni*, with every 10% increase in *Ni* leading to an average increase of 3.56% in *Nd'*. Thus, we conclude that *H'* and *Ni* are key factors influencing the nitrate contamination in groundwater near a subsurface cut-off wall.

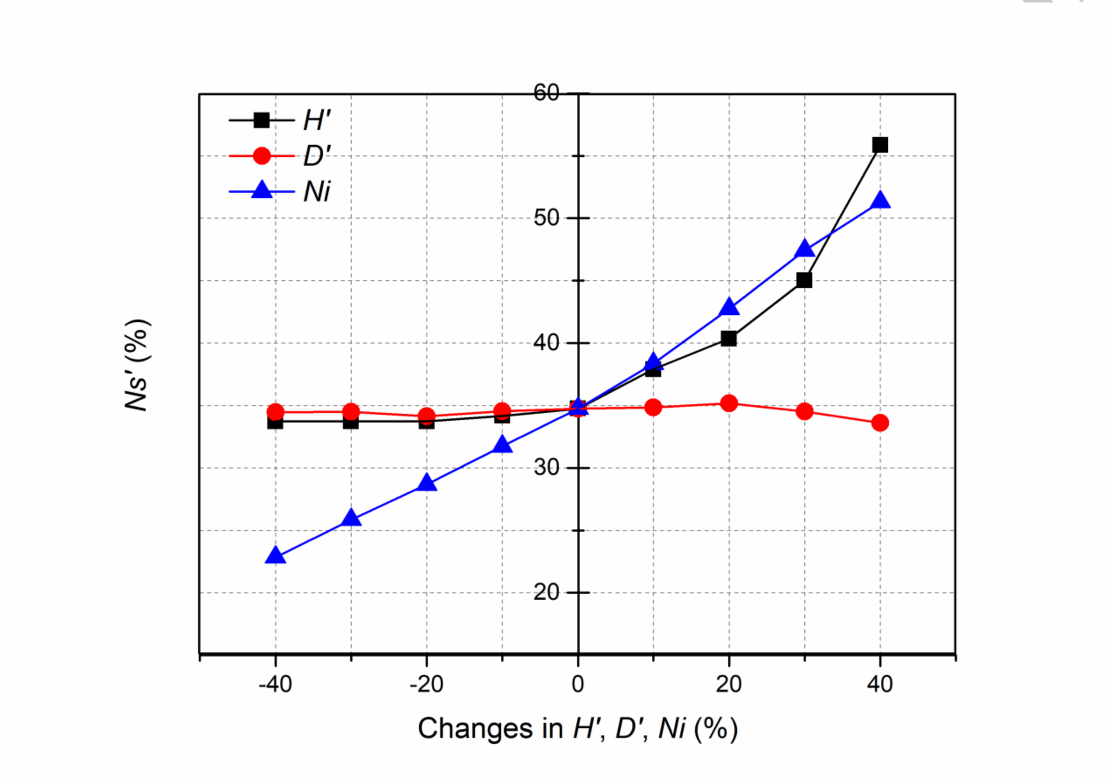

Fig. 16 Sensitivity of the steady-state relative nitrate contaminated area (*Ns'*) to the relative height of the subsurface cut-off wall (*H'*), the relative distance between the subsurface cut-off wall and Γ_s (*D'*), and nitrate infiltration rates (*Ni*). In the control, *H'*=65%, *D'*=25%, *Ni*=2.3 m/d.

Under SI conditions without a subsurface cut-off wall, a low-velocity zone (< 1 m/d) was formed due to the existence of the SW. Freshwater and nitrate migrated along the interface of the SW, forming a semi-elliptical pollution plume along the upper portion of the aquifer. The mean velocity in the domain was 2.24 m/d, and *Nd'* and *Ns'* were 52.5% and 33.82%, respectively. After constructing the cut-off wall, the flow pattern became more complicated. The area of the low-velocity zone (1–2 m/d) enlarged, the domain mean velocity decreased to 1.93 m/d, the nitrate-contaminated area expanded, and *Nd’* and *Ns’* increased to 54.68% and 34.58%, respectively. Further, the pollution plume caved inward just above the cut-off wall, the width of the transition zone increased, and the nitrate pollution plume became more diffuse as it approached the saltwater transition zone.

Changes in *H’* had little effect on the size of the saltwater-contaminated area but significantly influenced the nitrate distribution in groundwater; *Ns’* and *Ng* increased with increases in *H’*. We chose the height at which the cut-off wall was 80% of the thickness of the aquifer to be the critical height. When *H’* was lower than the critical height, *Ns’* slowly increased with respect to an increase in *H’* . When *H’* was higher than the critical height, *Ns’* increased rapidly--13.98% on average for a 10.00% increase in *H’*. Therefore, we suggest that subsurface cut-off walls be designed such that their height is less than or equal to the critical height to avoid enlargement of the nitrate-contaminated area in groundwater.

Changes in *D’* had a minor impact on the groundwater nitrate contamination but significantly influenced the size of the saltwater-contaminated area, which expanded with increases in *D’*. *Nd’* decreased with increasing *D’*, *Ns’* slightly decreased, and *Ng* hardly changed. Considering the dual effects of the subsurface cut-off wall on SI prevention and nitrate contamination, we suggest that the subsurface cut-off wall be constructed to control SI and be less than or equal to the critical height.

Changes in *Ni* had little effect on the saltwater-contaminated area but had a significant effect on *Nd’*, *Ns’*, and *Ng*. *Nd’* showed a linear increase with increases in *Ni*; a

10% increase in *Ni* led to a 4.12% increase in *Nd'*. When *Ni* was lower than 2.76 m/d, *Ns'* increased linearly, with an average increase of 2.74% for a 10% increase in *Ni*. However, when *Ni* was greater than 2.76 m/d, *Ns'* increased rapidly, with a 10% increase in *Ni* leading to a 4.28% increase in *Ns'*, on average. The increases in *Ng* were also accelerated when *Ni* was more than 2.76 m/d. Thus, reducing the infiltration rate by using water-saving irrigation techniques would be an effective way to prevent the spread of nitrate contamination in groundwater near a subsurface cut-off wall.

In field applications, the dual effects of the height of the subsurface cut-off wall on the SI and nitrate contamination in groundwater should be considered in the wall's construction. The minimum height of the cut-off wall should be based on the height of SW where the wall is constructed. Typically, the subsurface cut-off wall is constructed close to the shoreline to increase the aquifer area, but that increases the height of the wall and leads to nitrate contamination in the aquifer. Therefore, the cut-off wall should be constructed at a location such that its height is both less than the critical height and is able to control SI. In this way, the wall can both control SI and reduce nitrate contamination.

In the future, we plan to perform studies that take denitrification and evaporation processes into account. Field denitrification kinetics will be studied, and hydrogeological parameters will be measured to set up a field-scale model and enhance the practical applicability of the theory developed herein.

Acknowledgements

The authors would like to thank the Key Project of Natural Science Foundation of China (No.41731280) and the Key Project of NSFC-Shandong Province Joint Funds

(No.U1806210) for funding this project.

6. References

Abarca, E., Prabhakar Clement, T., 2009. A novel approach for characterizing the mixing zone of a saltwater wedge. Geophys. Res. Lett. 36, 1–5. https://doi.org/10.1029/2008GL036995

Abdoulhalik, A., Ahmed, A., Hamill, G.A., 2017. A new physical barrier system for seawater intrusion control. J. Hydrol. 549, 416–427. https://doi.org/10.1016/j.jhydrol.2017.04.005

Abdoulhalik, A., Ahmed, A.A., 2017a. How does layered heterogeneity affect the ability of subsurface dams to clean up coastal aquifers contaminated with seawater intrusion? J. Hydrol. 553, 708–721. https://doi.org/10.1016/j.jhydrol.2017.08.044

Abdoulhalik, A., Ahmed, A.A., 2017b. The effectiveness of cutoff walls to control saltwater intrusion in multi-layered coastal aquifers: Experimental and numerical study. J. Environ. Manage. 199, 62–73. https://doi.org/10.1016/j.jenvman.2017.05.040

Ahmed, A.T., 2017. Experimental and numerical study for seawater intrusion remediation in heterogeneous coastal aquifer. J. Environ. Manage. 198, 221–232. https://doi.org/10.1016/j.jenvman.2017.04.055

Allow, K.A., 2012. The use of injection wells and a subsurface barrier in the prevention of seawater intrusion: A modelling approach. Arab. J. Geosci. 5, 1151–1161. https://doi.org/10.1007/s12517-011-0304-9

Bosello, F., De Cian, E., 2014. Climate change, sea level rise, and coastal disasters. A review of modeling practices. Energy Econ. 46, 593–605. https://doi.org/10.1016/j.eneco.2013.09.002

Botero-Acosta, A., Donado, L.D., 2015. Laboratory Scale Simulation of Hydraulic Barriers to Seawater Intrusion in Confined Coastal Aquifers Considering the Effects of Stratification. Procedia Environ. Sci. 25, 36–43. https://doi.org/10.1016/j.proenv.2015.04.006

Burow, K.R., Nolan, B.T., Rupert, M.G., Dubrovsky, N.M., 2010. Nitrate in groundwater of the United States, 1991-2003. Environ. Sci. Technol. 44, 4988–4997. https://doi.org/10.1021/es100546y

Chang, S.W., Clement, T.P., 2013. Laboratory and numerical investigation of transport processes occurring above and within a saltwater wedge. J. Contam. Hydrol. 147, 14–24. https://doi.org/10.1016/j.jconhyd.2013.02.005

Chen, S., Wu, W., Hu, K., Li, W., 2010. The effects of land use change and irrigation water resource on nitrate contamination in shallow groundwater at county scale. Ecol. Complex. 7, 131–138. https://doi.org/10.1016/j.ecocom.2010.03.003

Davidson, J., Good, C., Williams, C., Summerfelt, S.T., 2017. Evaluating the chronic effects of nitrate on the health and performance of post-smolt Atlantic salmon Salmo salar in freshwater recirculation aquaculture systems. Aquac. Eng. 79, 1–8. https://doi.org/10.1016/j.aquaeng.2017.08.003

Du, L. feng, Zhao, T. ke, Zhang, C. jun, An, Z. zhuang, Wu, Q., Liu, B. cun, Li, P., Ma, M. ting, 2011. Investigations on Nitrate Pollution of Soil, Groundwater and Vegetable from Three Typical Farmlands in Beijing Region, China. Agric. Sci. China 10, 423–430. https://doi.org/10.1016/S1671-2927(11)60021-7

Ferguson, G., Gleeson, T., 2012. Vulnerability of coastal aquifers to groundwater use and climate change. Nat. Clim. Chang. 2, 342–345.

Hans-Jörg G.Diersch, n.d. Finite Element Modeling of Flow,Mass and Heat Transport in Porous and Fractured Media. Springer Berlin Heidelberg.

Hu, K., Huang, Y., Li, H., Li, B., Chen, D., White, R.E., 2005. Spatial variability of shallow groundwater level, electrical conductivity and nitrate concentration, and risk assessment of nitrate contamination in North China Plain. Environ. Int. 31, 896–903. https://doi.org/10.1016/j.envint.2005.05.028

Hu, R., Zheng, X., Xin, J., Sun, Z., Zheng, T., 2017. Selective enhancement and verification of woody biomass digestibility as a denitrification carbon source. Bioresour. Technol. 244, 313–319. https://doi.org/10.1016/j.biortech.2017.07.162

Hussain, M.S., Javadi, A.A., Sherif, M.M., 2015. Three dimensional simulation of seawater intrusion in a regional coastal aquifer in UAE. Procedia Eng. 119, 1153–1160. https://doi.org/10.1016/j.proeng.2015.08.965

Ishida, S., Motoku, M., Abe, E., Fazal, M.A., Tsuchihara, T., Imaizumi, M., 2003. Construction of subsurface dams and their impact on the environment. RMZ- Mater. Geoenvironment 50, 149–152.

Kaleris, V.K., Ziogas, A.I., 2013. The effect of cutoff walls on saltwater intrusion and groundwater extraction in coastal aquifers. J. Hydrol. 476, 370–383. https://doi.org/10.1016/j.jhydrol.2012.11.007

Kang, P., Xu, S., 2017. The impact of an underground cut-off wall on nutrient dynamics in groundwater in the lower Wang River watershed, China. Isotopes Environ. Health Stud. 53, 36–53. https://doi.org/10.1080/10256016.2016.1186670

Kringel, R., Rechenburg, A., Kuitcha, D., Fouépé, A., Bellenberg, S., Kengne, I.M., Fomo, M.A.,

2016. Mass balance of nitrogen and potassium in urban groundwater in Central Africa, Yaounde/Cameroon. Sci. Total Environ. 547, 382–395. https://doi.org/10.1016/j.scitotenv.2015.12.090

Lalehzari, R., Tabatabaei, S.H., 2015. Simulating the impact of subsurface dam construction on the change of nitrate distribution. Environ. Earth Sci. 74, 3241–3249. https://doi.org/10.1007/s12665-015-4362-2

Lu, J., Bai, Z., Velthof, G.L., Wu, Z., Chadwick, D., Ma, L., 2019. Accumulation and leaching of nitrate in soils in wheat-maize production in China. Agric. Water Manag. 212, 407–415. https://doi.org/10.1016/j.agwat.2018.08.039

Luyun, R., Momii, K., Nakagawa, K., 2009. Laboratory-scale saltwater behavior due to subsurface cutoff wall. J. Hydrol. 377, 227–236. https://doi.org/10.1016/j.jhydrol.2009.08.019

Post, V., Kooi, H., Simmons, C., 2007. Using hydraulic head measurements in variable-density ground water flow analyses. Ground Water 45, 664–671. https://doi.org/10.1111/j.1745-6584.2007.00339.x

Radfard, M., Rahmatinia, M., Solimani, H., jazari, M.D., Mahvi, A.H., Azhdarpoor, A., 2018. Data on health risk assessment to the nitrate in drinking water of rural areas in the Khash city, Iran. Data Br. 21, 1918–1923. https://doi.org/10.1016/j.dib.2018.11.007

Rajmohan, N., Al-Futaisi, A., Al-Touqi, S., 2009. Geochemical process regulating groundwater quality in a coastal region with complex contamination sources: Barka, Sultanate of Oman. Environ. Earth Sci. 59, 385–398. https://doi.org/10.1007/s12665-009-0037-1

Rodriguez-Galiano, V.F., Luque-Espinar, J.A., Chica-Olmo, M., Mendes, M.P., 2018. Feature selection approaches for predictive modelling of groundwater nitrate pollution: An evaluation of filters, embedded and wrapper methods. Sci. Total Environ. 624, 661–672. https://doi.org/10.1016/j.scitotenv.2017.12.152

Rojas Fabro, A.Y., Pacheco Ávila, J.G., Esteller Alberich, M.V., Cabrera Sansores, S.A., Camargo-Valero, M.A., 2015. Spatial distribution of nitrate health risk associated with groundwater use as drinking water in Merida, Mexico. Appl. Geogr. 65, 49–57. https://doi.org/10.1016/j.apgeog.2015.10.004

Shammas, M.I., Thunvik, R., 2009. Predictive simulation of flow and solute transport for managing the Salalah coastal aquifer, Oman. Water Resour. Manag. 23, 2941–2963. https://doi.org/10.1007/s11269-009-9417-2

Singh, A., 2015. Managing the environmental problem of seawater intrusion in coastal aquifers through simulation-optimization modeling. Ecol. Indic. 48, 498–504. https://doi.org/10.1016/j.ecolind.2014.09.011

Smith, A.J., 2004. Mixed convection and density-dependent seawater circulation in coastal aquifers. Water Resour. Res. 40, 1–16. https://doi.org/10.1029/2003WR002977

Srivastava, S.K., Ramanathan, A.L., 2018. Geochemical assessment of fluoride enrichment and nitrate contamination in groundwater in hard-rock aquifer by using graphical and statistical methods. J. Earth Syst. Sci. 127, 1–23. https://doi.org/10.1007/s12040-018-1006-4

van den Brink, C., Frapporti, G., Griffioen, J., Zaadnoordijk, W.J., 2007. Statistical analysis of anthropogenic versus geochemical-controlled differences in groundwater composition in The Netherlands. J. Hydrol. 336, 470–480. https://doi.org/10.1016/j.jhydrol.2007.01.024

Volker, R.E., Zhang, Q., Lockington, D.A., 2002. Numerical modelling of contaminant transport in coastal aquifers. Math. Comput. Simul. 59, 35–44. https://doi.org/10.1016/S0378-4754(01)00391-3

Wang, L., Zheng, X., Tian, F., Xin, J., Nai, H., 2018. Soluble organic nitrogen cycling in soils after application of chemical/organic amendments and groundwater pollution implications. J. Contam. Hydrol. 217, 43–51. https://doi.org/10.1016/j.jconhyd.2018.08.003

Werner, A.D., Bakker, M., Post, V.E.A., Vandenbohede, A., Lu, C., Ataie-Ashtiani, B., Simmons, C.T., Barry, D.A., 2013. Seawater intrusion processes, investigation and management: Recent advances and future challenges. Adv. Water Resour. 51, 3–26. https://doi.org/10.1016/j.advwatres.2012.03.004

Wu, J., Ding, J., Lu, J., 2016. Nitrate Transport Characteristics in the Soil and Groundwater. Procedia Eng. 157, 246–254. https://doi.org/10.1016/j.proeng.2016.08.363

Xin, J., Tang, F., Zheng, X., Shao, H., Kolditz, O., Lu, X., 2016. Distinct kinetics and mechanisms of mZVI particles aging in saline and fresh groundwater: H2evolution and surface passivation. Water Res. 100, 80–87. https://doi.org/10.1016/j.watres.2016.04.074

Xin, P., Li, L., Shen, C., Lu, C., Kong, J., Zhang, C., Zhao, Z., 2019. Solute transport influenced by unstable flow in beach aquifers. Adv. Water Resour. 125, 68–81. https://doi.org/10.1016/j.advwatres.2019.01.009

Yoshimoto, S., Tsuchihara, T., Ishida, S., Imaizumi, M., 2013. Development of a numerical model for nitrates in groundwater in the reservoir area of the Komesu subsurface dam, Okinawa, Japan. Environ. Earth Sci. 70, 2061–2077. https://doi.org/10.1007/s12665-

011-1356-6

Zhang, Q., Volker, R.E., Lockington, D.A., 2002. Experimental investigation of contaminant transport in coastal groundwater. Adv. Environ. Res. 6, 229–237. https://doi.org/10.1016/S1093-0191(01)00054-5

Zhang, Q., Volker, R.E., Lockington, D.A., 2001. Influence of seaward boundary condition on contaminant transport in unconfined coastal aquifers. J. Contam. Hydrol. 49, 201–215. https://doi.org/10.1016/S0169-7722(00)00194-7

Zhang, W.L., Tian, Z.X., Zhang, N., Li, X.Q., 1996. Nitrate pollution of groundwater in northern China. Agric. Ecosyst. Environ. 59, 223–231. https://doi.org/10.1016/0167-8809(96)01052-3